Dual Doppler Radar Analysis of a Tornadic Quasi-Linear Convective System on 04 January 2015

DUSTIN CONRAD, KEVIN KNUPP, ANTHONY LYZA, AND CARTER HULSEY

Department of Atmospheric Science, University of Alabama-Huntsville, Huntsville, AL

1. Introduction

This study examines a tornadic quasi-linear convective system (QLCS) that occurred on 04 January, 2015. The system produced an EF-1 tornado for 10.3 km along the northern edge of the city of Albertville, AL from 0140 UTC to 0206 UTC. The tornado occurred in the southern dual-Doppler lobe of the University of Alabama-Huntsville's Advanced Radar for Meteorological and Observational Research (ARMOR) and the National Weather Service Weather Surveillance Radar 1988-Doppler (WSR-88D) in Hytop, AL (KHTX) (Figure 1).

The tornado occurred in a high shear-low CAPE (HSLC) environment, with surface based CAPE near 38 J/kg and 0-3 km (0-1 km) near 50 kts (41 kts) (Figure 2). A stout wind shift was present along the leading edge of the QLCS, leading to the hypothesis of horizontal shearing instability (HSI) as the primary vortexgensis mechanism. Previous studies have proposed different methods of vortex formation within QLCSs that involve tilting of downward vorticity along the top of the cold pool (Trapp and Weismann 03; hereafter TW03), upward tilting of horizontal vorticity along the leading edge of the cold pool (Atkins and St. Laurent 09b; hereafter AS09), downward tilting of baroclinic vorticity early in the QLCS's life cycle behind the gust front (TW03), and upward tilting of preexisting horizontal vorticity not created by the cold pool (AS09). Clark and Parker 14 (hereafter CP14) performed an analysis of multiple tornadic and non-tornadic narrow cold frontal rainbands over the United Kingdom and found that rainbands with a strong wind shift and strong flow behind the leading edge were typically tornadic, while others were not. CP14 found that:

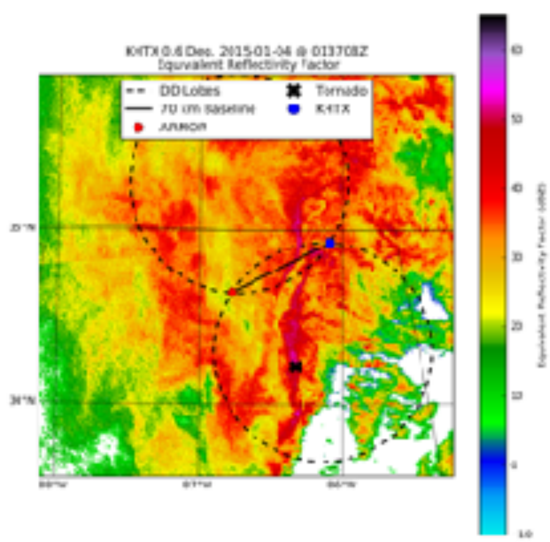

Figure 1: Graphical display of southeastern dual-Doppler lobe between ARMOR and KHTX. Black x represents location of the tornado.

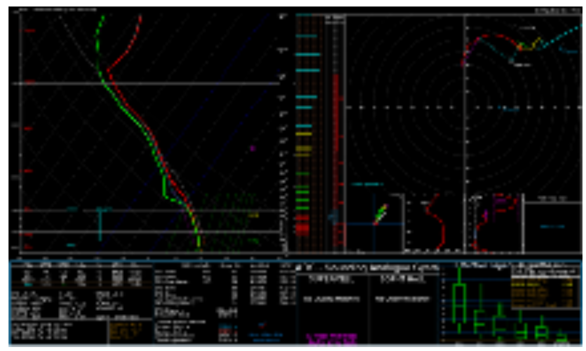

Figure 2: RAP sounding for Albertville, AL. No in situ soundings were performed during this event and next closest observed sounding was not representative of wind profile in which the tornado occurred. Sounding reveals 50 kts of surface-3 km shear and 41 kts of surface- 1km shear in addition to 38 J/kg of surface based CAPE.

- *Wind Shift >> 45° and strong post-frontal winds were all tornadic*
- *Wind Shift <= 45° and strong post-frontal winds were non-tornadic*
- *Weak post-frontal winds were not conducive for tornadoes*

Ahead of the QLCS, small segments of reflectivity were propagating perpendicular to the leading edge of the QLCS and faster than the background flow. It is hypothesized that these reflectivity segments are indicative of an atmospheric wave. Coleman and Knupp 08 (hereafter CK08) showed how wave interactions with mesocyclones can lead to an intensification of the mesocyclone and can potentially lead to tornadogenesis. Following vortexgenesis, the reflectivity segments propagated

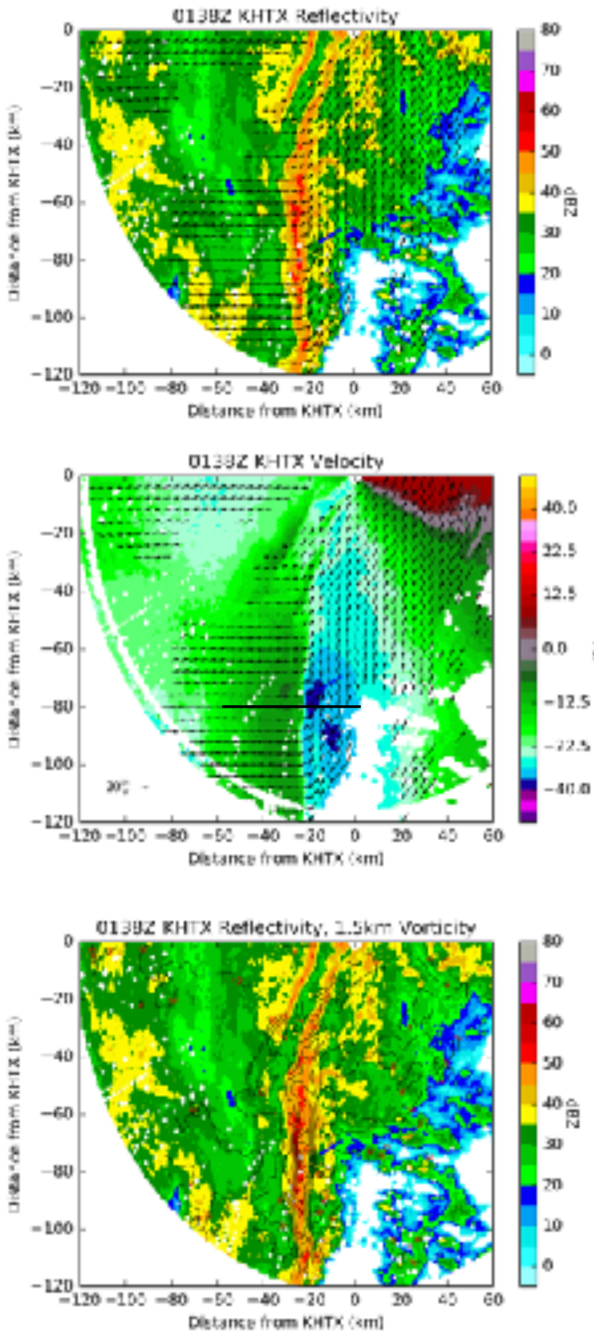

Figure 3: Objectively-analyzed radar reflectivity factor (top), vorticity (middle) and radial velocity (m s-1; bottom) from KHTX at 0138 UTC at 1500 m above ground level (AGL). Vorticity is contoured at an interval of 1x10-3 s-1. At this time, there were strong pre- and post-QLCS winds with a wind shift of almost 90° at the gust front. The tornadic vortex is located near (x = -25 km, y = -78 km). Blue line indicates tornado track.

through the northern vortex leading to an intensification. This did not occur for the southern mesovortex.

Two separate analyses at different times will be performed to study the role of HSI in mesovortexgenesis. An analysis of the favorability of the environment to wave formation/maintenance will also be performed. A brief summary of the data and methodology will be presented in section 2. Dual-Doppler analysis of the QLCS for the two separate times will be performed in section 3. The wave analysis will be given in section 4. A brief summary and conclusions will be presented in section 5.

2. Data and Methodology

The ARMOR radar is a C-band (5.5 cm) wavelength radar with dual-polarization capabilities. The beam width is 1.0° and was operating in a 5-tilt rain one strategy with elevation angles at 0.7°, 1.3°, 2.0°, 2.7°, and 3.4°. KHTX is an S-band (10 cm) wavelength radar operated by the NWS in Huntsville, AL. The beam width is 0.95° and was operated in VCP 212. Data were edited using Solo3 software. Areas of ground clutter and noise were manually determined from the reflectivity, radial velocity, and correlation coefficient (RHOHV) fields and were removed. Manual unfolding of radial velocity was performed on ARMOR and KHTX.

Data were mapped to a regular Cartesian grid using a Cressman analysis. A 1-point linear interpolation was used. For all analyses, the horizontal grid spacing is 1000 m and the vertical grid spacing is 500 m. Dual-Doppler wind syntheses were performed using CEDRIC. To reduce errors in the DD analyses, only ARMOR volume scans that were fully within a KHTX volume scan were used for the wind syntheses.

3. Dual Doppler Analysis

a) Tornadic Vortex

In order to determine if HSI was the main mechanism for vortexgenesis, the analysis of the tornadic vortex will occur at 0138 UTC, the radar volume shortly before tornadogenesis. Figure 3 depicts dual-Doppler winds overlaid on horizontal reflectivity from KHTX, dual-Doppler winds overlaid on radial velocity from KHTX, and vertical vorticity contoured over horizontal reflectivity from KHTX. Vorticity is contoured at $1x10^{-3}$ s^{-1}. All three images were taken at 1.5 km above ground level (AGL) as this was the lowest vertical distance in which both vortices had dual-Doppler winds. The blue line in both figures indicates the track of the tornado.

Along the leading edge of the QLCS, a wind shift of near 90° is present and as a result a vertical vortex sheet has formed. Winds ahead and behind the leading edge of the QLCS are strong, with magnitudes greater than 20 m/s. Thus, our results line up well with what was observed in CP14, with a wind shift >> 45° and strong pre- and post-QLCS winds.

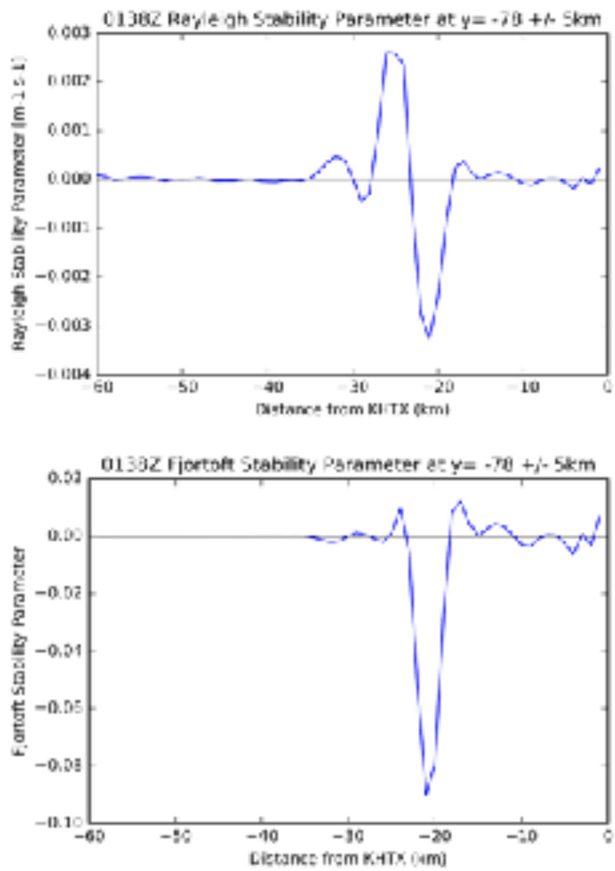

Figure 4: Rayleigh and Fjortoft stability criteria calculated along black line through the tornadic vortex (78 km south of KHTX) in velocity image above. $\overline{v}$ is average meridional wind and $\overline{v}$# is meridional wind at the inflection point. Change in sign of Rayleigh stability criterion indicates inflection point is present and is necessary but insufficient condition for horizontal shear instability (HSI) to occur. Negative Fjortoft parameter reveals that the vortex is not near the boundaries (Marchioro and Pulvirenti 1994) and is also necessary but insufficient for HSI.

The vertical vortex sheet has a magnitude of around $2x10^{-3}$ s^{-1}, with the strongest areas of vertical vorticity associated with the tornado and the non-tornadic vortex. The tornadic vortex has a magnitude of $6x10^{-3}$ s^{-1}.

In order for HSI to occur, two stability criterion have to be met as shown in Marchioro and Pulvirenti 94. The first criteria is the presence of an inflection point, as found by Lord Rayleigh. An inflection point is present when $\partial^2\overline{v}/\partial x^2 = 0$, where $\overline{v}$ is the average component of the wind parallel to the leading edge of the flow. Therefore, the presence of an inflection point will be shown when the Ryaliegh criteria changes sign. Since this is a N-S orientated QLCS, the change in $\overline{v}$ will be take in respect to a change in x. To mitigate the impacts of the tornadic circulation, the average of the v-component of the winds was taken over 10 km length, 5 km N and S of the vortex center. The second criteria is that the inflection point be away from the boundaries set in the derivation of the Rayleigh criteria (shown in Marchioro and Pulvirenti 94). This criteria is known as the Fjortoft criteria and is met when $\partial^2\overline{v}/\partial x^2(\overline{v} - \overline{v}_I)$ is below 0 somewhere in the flow, where $\overline{v}_I$ is the flow at the inflection point.

Figure 4 displays the Rayleigh and Fjortoft parameters for the 0138 UTC time. These have been calculated along the black lines in Figure 3. The Rayleigh criteria for this time has been met as indicated by the large change in sign centered on -22 km from KHTX. The Fjortoft criteria is also met for this time given the large negative spike highlighted by the black box. The peak to 0 within the large negative spike is a result of subtracting the flow at the inflection point from itself.

Since both of the major criteria for HSI have been met, it is likely that the vortex associated with the tornado was created by HSI. However, both of these criteria are necessary for HSI but are insufficient for HSI. Therefore, HSI cannot be definitely ruled as the main formation mechanism for this vortex.

b) Nontornadic Vortex

South of the tornadic vortex and at 0149 UTC, another non-tornadic vortex formed. As with the prior time, this vortex formed along a stout wind shift in a similar time scale similar to the tornadic vortex. This non-tornadic vortex is also hypothesized to have formed as a results of HSI. Figure 5 depicts dual-Doppler winds overlaid on horizontal reflectivity from KHTX, dual-Doppler winds overlaid on radial velocity from KHTX, and vertical vorticity contoured over horizontal reflectivity from KHTX. Vorticity is contoured at 1x10-3 s-1. All three images were taken at 1.5 km above ground level (AGL).

As with before, a wind shift of near 90° exists along the leading edge, although for this later time this change take place over a slightly larger x-distance. The magnitude of the winds behind and ahead of the leading edge of the QLCS are similar to before, with magnitudes near or greater than 20 m/s. For this southern vortex, the QLCS is in line with the results given in CP14 that this should be a tornadic vortex, yet there was no tornado associated with it. This will be addressed in section 4.

Figure 6 depicts the Rayleigh and Fjortoft stability criterion for HSI. These were analyzed along the black lines in Figure 5. The change in sign in the Ryaliegh criteria is highlighted by the black line and the negative spike in the Fjortoft criteria is highlighted by the black box. Thus, both the Rayleigh and Fjortoft criterion are satisfied for this time period as with before. However, the magnitude for this second vortex is lower than what is seen at 0138Z. Thus, it is likely that this southern vortex is also formed as a result of HSI.

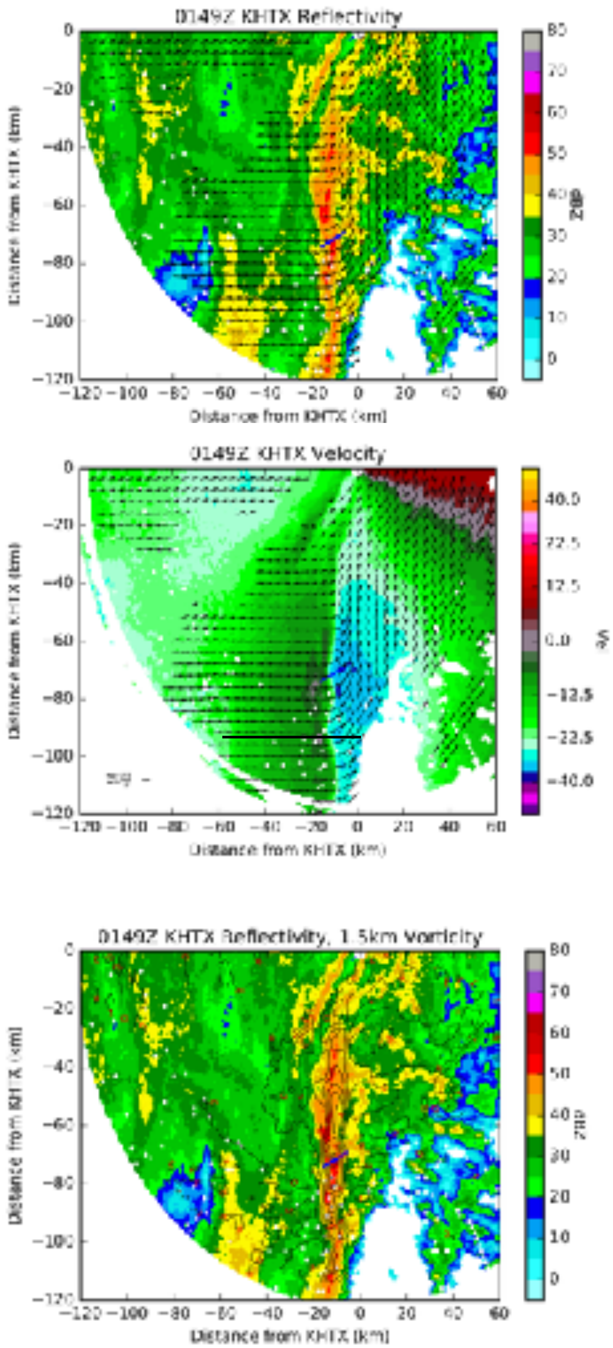

Figure 5: Objectively-analyzed radar reflectivity factor (top), vorticity (middle) and radial velocity (m s-1; bottom) from KHTX at 0149 UTC at 1500 m above ground level (AGL). Vorticity is contoured at an interval of 1x10-3 s-1. Wind shift is broader with slightly weaker winds ahead of the QLCS. Nontornadic vortex is located near (x = -18 km, y = -93 km). Blue line indicates tornado track.

4. Wave Analysis

To this point, it has been shown that both vortices likely have formed due to HSI. However, the reason why the northern vortex became tornadic and the southern one did not has not been solved. It is hypothesized that an interaction with a gravity wave like feature is responsible for the increase in mesocyclone strength, similar to what is seen in CK08. It is hypothesized that this wave like feature interacted with the positive updraft perturbation associated with the vortex created by the HSI and tilted and subsequently stretched the horizontal vorticity along the wave to form the tornado.

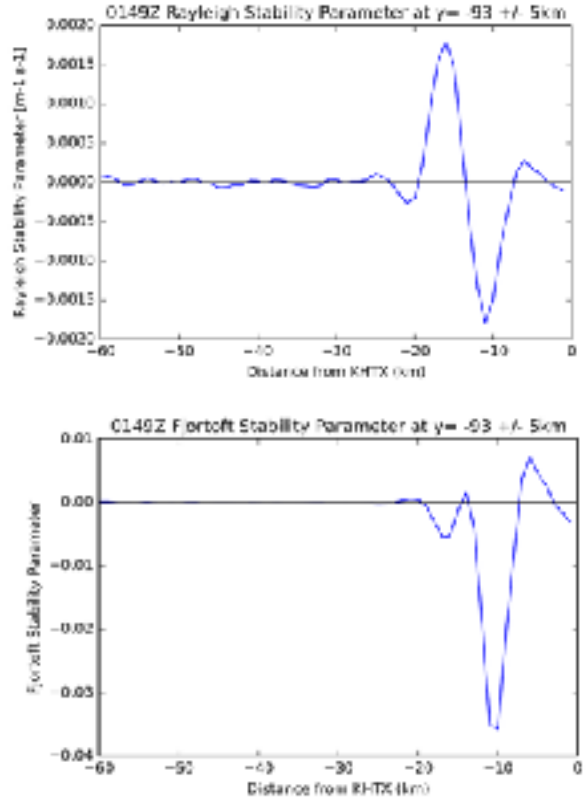

Figure 6: Rayleigh and Fjortoft stability criteria calculated along black line through the nontornadic vortex (93 km south of KHTX) in velocity image above. $\overline{v}$ is average meridional wind and $\overline{v}\#$ is meridional wind at the inflection point. Change of sign in Rayleigh stability criterion and negative values of Fjortoft stability criterion are necessary but insufficient conditions for HSI. Magnitude of criteria at this time are less than that of the northern vortex.

Horizontal vorticity was calculated from the dual-Doppler winds. Given that ARMOR was only in a 5-tilt low levels only strategy, accurate representation of vertical velocity was not obtained. Therefore, the horizontal field shown in Figure 7 will only be used in a quantitive sense. The 0138 UTC volume was selected as this was the time period in which the wave interacted with the vortex. Along the leading edge of the wave, areas of horizontal vorticity are present, lending some support that this is a wave feature of some sort. Due to lack of high resolution, low level dual-Doppler and an absence of surface stations, radar or ground validation of the wave feature is not possible.

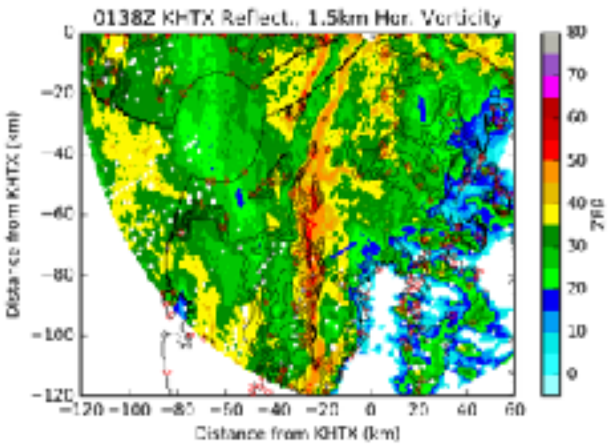

Figure 7: Objectively-analyzed radar reflectivity factor from KHTX at 1.5 km AGL at 0138 UTC. Horizontal vorticity is contoured at an interval of 1x10-3 s-1. The quasi-linear light reflectivity structures may have been caused by gravity waves; quantitative analysis regarding the presence of these waves can be found to the right. Blue line indicates tornado track.

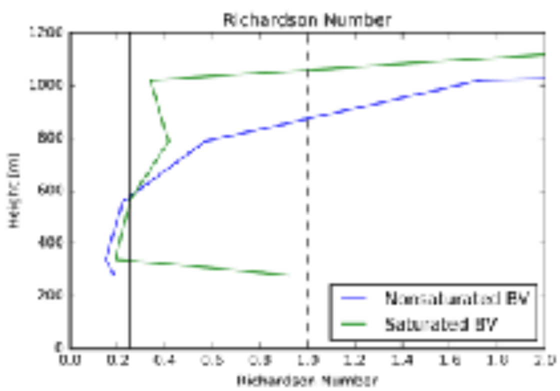

Figure 8: Profile of Richardson Number calculated from the RAP sounding using saturated and non-saturated Brunt-Vaisala frequency. Values below 0.25 (1.0) are supportive for generation (maintenance) of Kelvin-Helmholtz waves. u is wind speed in direction of wave motion.

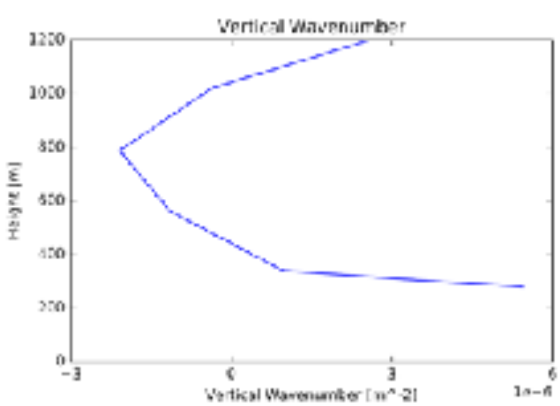

Figure 8: Profile of vertical wavenumber determined from Eq 1 using RAP sounding. Gravity waves can be reflected by the ground and by layers of decreasing m2 (CK08). u is wind speed in direction of wave motion.

Instead, the environment will be analyzed using the RAP sounding (Figure 2) to see if it is conducive for the generation or maintenance of gravity waves or Kelvin-Helmholtz (KH) type waves. In order to provide confidence in the use of the RAP sounding, a comparison with the nearest 00 UTC sounding in Birmingham, AL was performed (not shown). Thermodynamic profiles were similar except for differences in surface conditions, which observations seen in the RAP are close to what was observed at the UAH berm surface observing station. Wind profiles from the UAH Mobile Integrated Profiling System 915 MHz wind profiler were in good agreement with what was seen in the RAP sounding as well (not shown).

Two possible wave types will be investigated, a KH wave and a ducted gravity wave. KH waves can be generated (maintained) in an environment in which the Richardson Number is below .25 (1) (Nappo 2013). Figure 8 shows profiles for the lowest 1200 m of the Richardson Number calculated with the dry and saturated Brunt-Vaisala frequencies. Given the saturated nature of the thermodynamic profile seen in the RAP sounding, using the saturated Brunt-Vaisala frequency is more appropriate. Throughout the lowest 1000 m, the environment is supportive of the maintenance of KH waves as the Richardson Number is below 1 for this whole level. A small layer starting at around 300 m extending to 550 m is also supportive for the generation of KH waves as well.

The second type of wave that will be investigated is a gravity wave. Ducted gravity waves are seen in environments in which the vertical wavenumber decrease with height (Nappo 2013). Figure 9 depicts the vertical wave number in the lowest 1200 m calculated from the RAP sounding. A decreasing layer near 300 m to 800 m can be seen, indicating that the environment may be supportive of a gravity wave, most likely due to the shear term in the vertical wave number equation:

$$m^2 = \frac{N^2}{(c-U)^2} - \frac{\frac{d^2U}{dz^2}}{(c-U)} - k^2 \qquad (1)$$

where the first term on the right hand side is the thermal stability term, followed by the shear curvature term, and the horizontal wave number squared. U is the environmental wind in the direction of the wave, c is the speed of the wave, and N is the Brunt-Vaisala frequency. The proximity of this decreasing layer of m^2 to the ground along with it becoming negative, which can be destructive of gravity waves due to resonance, leads to the hypothesis that the wave feature is more similar to a KH wave rather than a gravity wave. This is only a hypothesis however due to reasons from above.

5. Summaries and Conclusions

Dual-Doppler wind synthesis at two separate times reveal a well-defined wind shift located along the leading edge of the QLCS. The sharpness of the wind shift and pre- and post-QLCS intensity of the winds are consistent with the results of CP14, who demonstrated that a wind shift >> 45° and strong pre- and post-frontal winds in a narrow cold frontal rainband are supportive of tornadoes. Calculation of the Rayleigh Stability parameter shows that for both the northern and southern vortex, an inflection point was present. The more stringent Fjortoft Stability Parameter reveals that the relative maximum in vertical vorticity is away from the boundary (Marchioro and Pulvirenti 1994). Therefore, we hypothesize that HSI is the primary formation mechanism for these vortices.

Shortly before tornadogenesis, reflectivity structures propagate perpendicular to the leading edge of the QLCS. It is hypothesized that these segments are indicative of a wave-like feature, and the subsequent tilting of horizontal vorticity into the mesocyclone led to an increase in vertical vorticity and tornadogenesis. The environment depicted by the model sounding is supportive of the formation and maintenance of gravity and Kelvin-Helmholtz waves. A lack of surface observations over the area of interest, in addition to low resolution dual-Doppler data, does not allow for validation of a possible wave, however.

Similar analyses will be explored on other events that occurred within the North Alabama domain with improved radar coverage. Trajectory analyses will be performed with the Weather Research and Forecasting model to track parcel paths within the circulations and along the leading edge of potential wavelike features.

Acknowledgments: We thank Dr. Tim Coleman, Ryan Wade and Dr. Todd Murphy for their assistance and input with the wave analysis segment of this project and Dr. Jeff Frame for aiding with the HSI analysis. Barrett Goudeau and Austin Vacek are also acknowledge. Support from the Northern Gulf Institute Grant 191001.363513.04A is also acknowledged.

REFERENCES

Atkins, N. T., and M. St. Laurent, 2009: *Bow Echo Mesovortices. Part I: Processes That Influence Their Damaging Potential*. Mon. Wea. Rev., 137, 1497–1513.

Atkins, N. T., and M. St. Laurent, 2009: *Bow Echo Mesovortices. Part II: Their Genesis*. Mon. Wea. Rev., 137, 1514–1532.

Clark, M. R. and D. J. Parker, 2014: *On the mesoscale structure of surface wind and pressure fields near tornadic and nontornadic cold fronts*. Mon. Wea. Rev., 142, 3560– 3585, doi:10.1175/ MWR-D-13-00395.1.

Coleman, T. A., and K. R. Knupp, 2008: *The interactions of gravity waves with mesocyclones: Preliminary observations and theory*. Mon. Wea. Rev., 136, 4206–4219, doi: 10.1175/2008MWR2391.1.

Marchioro, C. and M. Pulvirenti. *Mathematical Theory of Incompressible Nonviscous Fluids*. Springer-Verlag, 1994.

Nappo, C. J. *Atmospheric Gravity Waves*. Academic Press, 2013

Schenkman, A. D., and M. Xue, 2016: *Bow Echo Mesovortices: A Review*. Atmos. Res., 170, 1-13.

Trapp, R. J., and M. L. Weisman, 2003: *Low-Level Mesovortices within Squall Lines and Bow Echoes. Part II: Their Genesis and Implications*. Mon. Wea. Rev., 131, 2804–2823.

Wakimoto, R. M., H. V. Murphey, C. A. Davis, and N. T. Atkins, 2006: *High Winds Generated by Bow Echoes Part II: The Relationship between the Mesovortices and Damaging Straight-Line Winds*. Mon. Wea. Rev., 134, 2813–2829.

Weisman, M. L., and R. J. Trapp, 2003: *Low-Level Mesovortices within Squall Lines and Bow Echoes. Part I: Overview and Dependence on Environmental Shear*. Mon. Wea. Rev., 131, 2779–2803.

Wheatley, D. M., and R. J. Trapp, 2008: *The Effect of Mesoscale Heterogeneity on the Genesis and Structure of Mesovortices within Quasi-Linear Convective Systems*. Mon. Wea. Rev., 136, 4220–4241.